Composite Structures 131 (2015) 616–624

Contents lists available at ScienceDirect

Composite Structures

journal homepage: www.elsevier.com/locate/compstruct

In-plane stiffness of the anisotropic multifunctional hierarchical honeycombs

Yongtao Sun [a,b], Bo Wang [b,c], Nicola Pugno [d,e,f], Bin Wang [a], Qian Ding [a,*]

[a] Department of Mechanics, Tianjin University, Tianjin 300072, China
[b] State Key Laboratory of Structural Analysis for Industrial Equipment, Dalian University of Technology, Dalian 116023, China
[c] Department of Engineering Mechanics, Dalian University of Technology, Dalian 116023, China
[d] Laboratory of Bio-Inspired & Graphene Nanomechanics, Department of Civil, Environmental and Mechanical Engineering, University of Trento, I-38123 Trento, Italy
[e] Center for Materials and Microsystems, Fondazione Bruno Kessler, I-38123 Trento, Italy
[f] School of Engineering and Materials Science, Queen Mary Univerisity of London, Mile End Road, London E1 4NS, UK

ARTICLE INFO

Article history:
Available online 10 June 2015

Keywords:
In-plane stiffness
Original anisotropic hexagonal honeycomb (OAHH)
Anisotropic multifunctional hierarchical honeycomb (AMHH)
Triangular honeycombs
Kagome honeycombs

ABSTRACT

The anisotropic hexagonal honeycomb is one of the common honeycombs. To increase its in-plane stiffness greatly, in this paper the anisotropic multifunctional hierarchical honeycomb (AMHH) is proposed. It is constructed by replacing the solid cell walls of the original anisotropic hexagonal honeycomb (OAHH) with the equal mass isotropic substructures, triangular or Kagome honeycombs. Two kinds of AMHH structures are proposed. One corresponds to the OAHH with 120° angles between the jointed cell walls, the other one corresponds to the OAHH with angles between the jointed cell walls different from 120°. Through Euler beam theory, the in-plane stiffness of these two kinds of AMHH is analyzed. Results show that the triangular honeycomb substructures could greatly increase the in-plane stiffness of the AMHH by 1.5 times or even more than 100 times, depending on the thickness-to-length ratio of the oblique cell wall of the OAHH. And the validation of the range for the thickness-to-length ratio of the oblique cell wall, which is related to the density of the OAHH, could reach to 0.1. The present theory could be used for designing new tailorable anisotropic hierarchical honeycomb materials for multifunctional applications.

1. Introduction

Due to their specific in-plane and out-of-plane mechanical properties and their potential multifunctional applications such as heat dissipation, thermal isolation, energy absorption, sound and vibration control etc., the low density two-dimensional hexagonal honeycomb structures, which are generally used as the core of the sandwich panels, are very attractive candidates for a variety of applications in many diverse fields. For example, the paper honeycombs can be used to make structural and cushioning components [1]; the metal honeycombs can be designed as the core of the heat sink for electronic devices where the combined heat dissipation and structural load capacity are necessary [2,3]. For applications in aerospace engineering, the pressure adaptive honeycomb could be a novel concept for smart morphing aircraft structures [4,5] and the superalloy honeycomb sandwich thermal protection systems have good heat shielding characteristics and thermostructural performances for hypersonic flight vehicles [6]. Regarding the applications in civil engineering, the honeycomb wave impeding barrier for pile foundations of the high-speed train viaduct can effectively mitigate the field vibration resulted from the passing trains [7]; the multi-layer energy dissipating panel, consisting of the polymer honeycomb and the viscoelastic solid material, could increase greatly both the shear resistance and the energy dissipation at contact surfaces for retrofitting semi-rigidly connected steel frames [8]. Besides, the hexagonal honeycomb sandwich panels also show desirable abilities for tailoring impact resistance for racing cars [9], low floor bus [10] and train application [11], for mitigating blast wave to protect structures from the high intensity dynamic loads created by explosions in air or water [12] and so on.

However, one disadvantage about the hexagonal honeycombs is that they have very lower in-plane stiffness, which hinders their multifunctional applications severely. One common way to increase the in-plane stiffness of the hexagonal honeycombs is to introduce the concept of hierarchy, whose crucial role playing on stiffness, strength and toughness of the natural and bio-inspired materials has received considerable attention in the past years [13–27]. To the authors' knowledge, Lakes [13] is the earliest scientist who analyzed the strength and stiffness of the hierarchical

* Corresponding author.
E-mail address: qding@tju.edu.cn (Q. Ding).

http://dx.doi.org/10.1016/j.compstruct.2015.06.020
0263-8223/

honeycombs and showed that marked improvement in compressive strength can be realized in hierarchical structures for low-density honeycombs. In recent years, by tailoring the geometrical layouts of the original regular hexagonal honeycombs, some new kinds of hierarchical honeycomb structures are proposed. Taylor et al. [28] introduced the functionally graded hierarchical honeycombs and numerically proved that with careful design of functionally graded unit cells it is possible to exceed, by up to 75%, the density specific modulus of conventional versions. By repeatedly replacing each three-edge vertex of a base hexagonal network with a similar but smaller hexagon of the same orientation, the group of Vaziri constructed the low-density isotropic [29] and anisotropic [30] hierarchical honeycombs, respectively. Combining analytical analysis and numerical simulation, their results show that the isotropic hierarchical honeycombs of first and second order can be up to 2.0 and 3.5 times stiffer than regular honeycomb at the same mass [29] and the anisotropic hierarchical honeycombs of first to fourth order can be 2.0–8.0 times stiffer and at the same time up to 2.0 times stronger than regular honeycomb at the same wall angle and the same overall average density [30].

To greatly increase the in-plane stiffness of the regular hexagonal honeycombs at both low density and intermediate relative density, the group of Pugno [31,32] proposed the multifunctional hierarchical honeycombs (MHH) by replacing the cell wall of the original regular hexagonal honeycombs (ORHH) with three kinds of equal-mass isotropic substructures, including triangular, Kagome and chiral honeycombs, respectively. Analytical results show that the triangular and Kagome substructures result in substantial improvements by one order or even three orders of magnitude on Young's and shear moduli of the MHH structure, depending on the cell-wall thickness-to-length ratio of the ORHH [32]. And the chiral honeycomb could also greatly (more than 10 times) improve the in-plane stiffness of the MHH by appropriately designing its geometry [31].

Majority of the above mentioned works on hierarchical honeycombs are focusing on the mechanical properties of the isotropic ones, and relatively little attention is paid on the anisotropic ones. To greatly increase the in-plane stiffness of the anisotropic hexagonal honeycombs (with uniform cell wall thickness), in this paper, analog to the isotropic MHH, the anisotropic multifunctional hierarchical honeycombs (AMHH) are proposed. They are constructed by replacing the cell walls of the original anisotropic hexagonal honeycombs (OAHH) with the equal-mass isotropic triangular or Kagome honeycomb substructures. Through Euler beam theory the relative in-plane Young's modulus of the AMHH are analyzed. Two kinds of AMHH structures are studied. One corresponds to the OAHH with 120° angles between the jointed cell walls, the other one corresponds to the OAHH with angles between the jointed cell walls different from 120°.

One point to note is that only in-plane stiffness of the anisotropic multifunctional hierarchical honeycombs (AMHH) is studied in this paper and the reason we employ the definition "multifunctional" here is to be analogous to the isotropic multifunctional hierarchical honeycombs (MHH) we proposed in Refs. [31,32]. In fact, the heat transfer and vibro-acoustic properties of the MHH and AMHH are being studied by us and the related results will be given in other two papers in the near future.

2. AMHH corresponding to the OAHH with 120° angles between the jointed cell walls

In this section, we study the AMHH corresponding to the OAHH with 120° angles between the jointed cell walls, i.e., the angles between the oblique walls and the horizontal line (the principal direction 1) are 30° (see Fig. 1a). In this case, the layouts of the AMHH structures are geometrically compatible, i.e., the connection between the honeycomb substructure cell walls is geometrical occlusive naturally (Fig. 1b).

2.1. AMHH with triangular honeycomb substructures

2.1.1. Basic theory

First of all, we consider the AMHH with isotropic triangular honeycomb substructures (Fig. 1). Fig. 1a is the OAHH with the cell wall thickness, the vertical cell wall length and the oblique cell wall length denoted by t_0, h_0 and l_0 ($h_0 \neq l_0$), respectively. Fig. 1b is the AMHH with the cell wall thickness, the vertical cell wall length and the oblique cell wall length denoted by t_1, h_0 and l_0, respectively. It is easy to see that both the vertical cell wall lengths and the oblique cell wall lengths of the OAHH and the AMHH are identical. Amplifications of the oblique and the vertical AMHH cell walls in Fig. 1b are shown in Fig. 1c and d respectively, in which the triangular cell wall length and thickness are denoted by t_t and l_t. The out-of-plane depth is a constant and is identical for both structures.

In this paper, we suppose that both the cell walls of the AMHH and the triangular honeycomb substructures are Euler beams. That is to say, under small deformations only bending of the cell walls of the AMHH structure and the triangular honeycomb substructures is considered, which requires that $t_1/h_0 < 0.2$, $t_1/l_0 < 0.2$ and $t_t/l_t < 0.2$ [33].

The geometries of Fig. 1c and d imply that

$$\begin{cases} l_0 = n_1 l_t \\ h_0 = n_2 l_t \end{cases} \tag{1}$$

where n_1 and n_2 are the numbers of the solid triangular lattice cell walls lying on the middle line of the oblique (with length l_0) and vertical (with length h_0) AMHH cell walls, respectively. Rearranging Eq. (1) gives

$$\begin{cases} l_t = \frac{l_0}{n_1} = \frac{h_0}{n_2} \\ \frac{n_2}{n_1} = \frac{h_0}{l_0} \end{cases} \tag{2}$$

To make sure the validation of the assumptions $t_1/h_0 < 0.2$ and $t_1/l_0 < 0.2$, we define the hierarchical length ratio, i.e., the ratio between l_t and $\min[h_0, l_0]$, as

$$\lambda = \frac{1}{n} = \frac{l_t}{l} \tag{3}$$

in which

$$n = \begin{cases} n_1 & h_0/l_0 > 1 \\ n_2 & h_0/l_0 < 1 \end{cases} \tag{4}$$

$$l = \begin{cases} l_0 & h_0/l_0 > 1 \\ h_0 & h_0/l_0 < 1 \end{cases} \tag{5}$$

Then, from Fig. 1c or d, according to the equal-mass principle, we can find $t_0 l - \frac{1}{2\sqrt{3}} t_0^2 = 3 \times \frac{1}{2}\left(t_t l_t - \frac{\sqrt{3}}{2} t_t^2\right) M$, which gives

$$\frac{t_t}{l_t} = \frac{1}{\sqrt{3}}\left[1 - \sqrt{1 - \frac{4\sqrt{3}}{3\lambda^2 M}\frac{t_0}{l}\left(1 - \frac{1}{2\sqrt{3}}\frac{t_0}{l}\right)}\right] \tag{6}$$

where

$$\frac{t_0}{l} = \begin{cases} \frac{t_0}{l_0} & \frac{h_0}{l_0} > 1 \\ \frac{t_0}{l_0}\frac{1}{h_0/l_0} & \frac{h_0}{l_0} < 1 \end{cases} \tag{7}$$

and M is the total number of half thickness triangular lattice cells in one AMHH cell wall with length l and it relates to n and N by (See Appendix A)

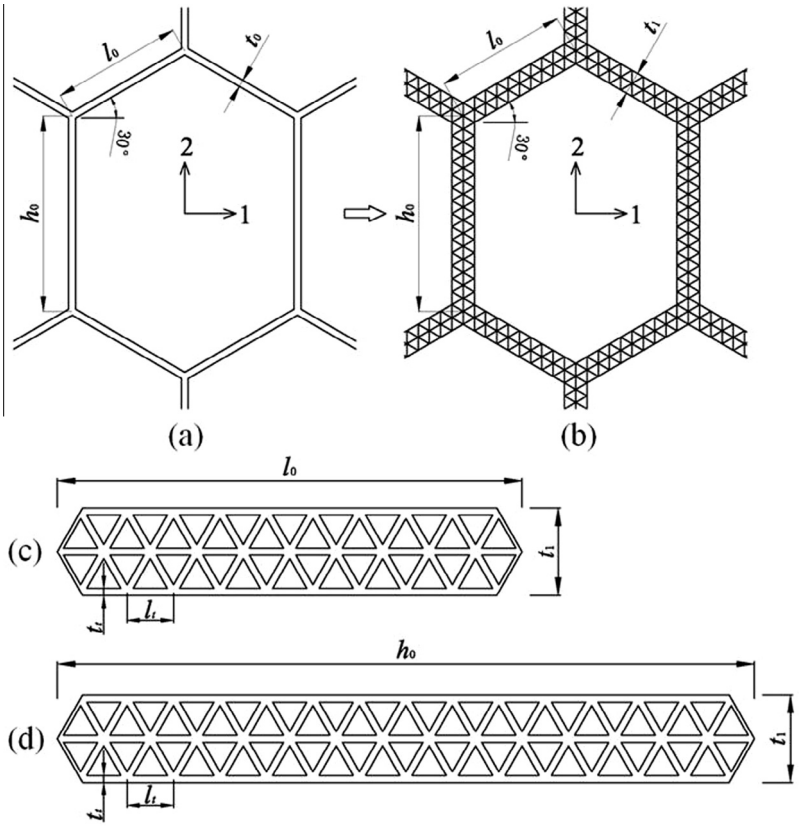

Fig. 1. Schematics of (a) the original anisotropic hexagonal honeycomb (OAHH) with 120° angles between the jointed cell walls; (b) the tailorable anisotropic multifunctional hierarchical honeycomb (AMHH) with triangular honeycomb substructures; (c) amplification of the oblique triangular lattice cell wall with length l_0 in (b); and (d) amplification of the vertical triangular lattice cell wall with length h_0 in (b).

$$M = 2N(2n - N) + \frac{2}{3}(n - N) \quad (1 \leqslant N \leqslant n) \tag{8}$$

in which N is the number of triangular lattice cells away from the middle line of the AMHH cell walls (e.g., in Fig. 1b $N = 1$). After this, from the precondition $t_t/l_t < 0.2$, we obtain $N_{\min}$, the lower bound of N:

$$N_{\min} = ce\left[\frac{6n - 1 - \sqrt{(6n-1)^2 - 12n\left[\frac{50}{10-\sqrt{3}} n \frac{t_0}{l}\left(1 - \frac{1}{2\sqrt{3}}\frac{t_0}{l}\right) - 1\right]}}{6}\right] \tag{9}$$

where 'ce[ ]' is the ceiling function, which denotes the smallest integer not less than the term in the bracket. Note that Eq. (9) may give $N_{\min} = 0$, in this case $N_{\min} = 1$.

On the other hand, from the geometrical analysis of Fig. 1c or d we get the cell wall thickness of the AMHH structure

$$t_1 = 2N\left(\frac{\sqrt{3}}{2} l_t\right) + t_t \tag{10}$$

that is

$$\frac{t_1}{l} = \left(\sqrt{3}N + \frac{t_t}{l_t}\right)\lambda \tag{11}$$

Then from the precondition $t_1/l < 0.2$, we obtain $N_{\max}$, the upper bound of N:

$$N_{\max} = fl\left[\frac{1}{5\sqrt{3}\lambda}\right] = fl\left[\frac{n}{5\sqrt{3}}\right] \tag{12}$$

where 'fl[ ]' is the floor function, which denotes the largest integer not greater than the term in the bracket.

Defining E_s as the Young's modulus of the solids of which the OAHH and the AMHH are made, E_t as the Young's modulus of the triangular honeycomb substructures, E_{O1}, E_{O2} as the Young's moduli of the OAHH in the principal directions 1 and 2, E_{M1}, E_{M2} as the Young's moduli of the AMHH in the principal directions 1 and 2, and by treating the substructure cell wall as a continuum, we find [33]:

$$\frac{E_t}{E_s} = \frac{2}{\sqrt{3}}\frac{t_t}{l_t} \tag{13}$$

$$\frac{E_{O1}}{E_s} = \frac{2\sqrt{3}}{h_0/l_0 + 1/2}\left(\frac{t_0}{l_0}\right)^3 \tag{14}$$

$$\frac{E_{M1}}{E_t} = \frac{2\sqrt{3}}{h_0/l_0 + 1/2}\left(\frac{t_1}{l_0}\right)^3 \tag{15}$$

$$\frac{E_{O2}}{E_s} = \frac{h_0/l_0 + 1/2}{3\sqrt{3}/8}\left(\frac{t_0}{l_0}\right)^3 \tag{16}$$

$$\frac{E_{M2}}{E_t} = \frac{h_0/l_0 + 1/2}{3\sqrt{3}/8}\left(\frac{t_1}{l_0}\right)^3 \tag{17}$$

where

$$\frac{t_1}{l_0} = \begin{cases} \frac{t_1}{l} & \frac{h_0}{l_0} > 1 \\ \frac{t_1}{l}\frac{h_0}{l_0} & \frac{h_0}{l_0} < 1 \end{cases} \tag{18}$$

Combining Eqs. (13)–(15) and Eqs. (13), (16), (17) gives the relative Young's moduli of the AMHH in the principal directions 1 and 2:

$$\frac{E_{M1}}{E_{O1}}=\frac{E_{M2}}{E_{O2}}=\frac{2}{\sqrt{3}}\frac{t_t}{l_t}\left(\frac{t_1}{l_0}\right)^3\Big/\left(\frac{t_0}{l_0}\right)^3 \tag{19}$$

t_1/l_0 in Eq. (19) has the form shown in Eq. (18).

One thing noteworthy is that the theory used in this paper, which treats the honeycomb substructures as a continuum, is related to the asymptotic homogenization of honeycomb structures, which are strictly valid for periodic cells in an infinite medium. In fact, for simplicity of the analysis of the elastic properties for periodic honeycomb structures, usually only one unit cell or even one quarter unit cell is chosen, whose elastic parameters are approximately treated as those for the whole periodic honeycomb structures [28,33]. From this point, the homogenized values of the in-plane stiffness of the honeycomb substructure, i.e., by treating the honeycomb substructures as a continuum, could be approximately valid, if only the cell sizes of the honeycomb substructures are small enough [13]. In this paper, the maximum value of the hierarchical length ratio λ is suggested to be 1/100, which for sure could guarantee the validation of the homogenization of the honeycomb substructures.

2.1.2. Effects of N and t_0/l_0 on the relative Young's moduli

To explicitly show how to design the AMHH structure with triangular honeycomb substructure under given parameters h_0/l_0 and t_0/l_0 of the OAHH structure and to investigate the effects of N and t_0/l_0 on the relative Young's moduli E_{M1}/E_{O1} and E_{M2}/E_{O2}, we consider the following examples with parameters $h_0/l_0=1.5,\ t_0/l_0=0.01,\ 0.02,\ 0.03,\ 0.04,\ 0.06,\ 0.08,\ 0.1$.

Since $h_0/l_0=1.5>1$, we could define $n_1=100,\ n_2=h_0/l_0n_1=150$ (See Eq. (2)). Then Eqs. (4), (5) and (3) give $n=n_1=100,\ l=l_0$ and $\lambda=1/n=l_t/l_0=1/100$, respectively. Through these parameters we could obtain $N_{\max}=11$ by Eq. (12) and the lower bound $N_{\min}$ for each t_0/l_0 by Eq. (9). The relative Young's moduli E_{M1}/E_{O1} and E_{M2}/E_{O2} vs. N for all the t_0/l_0 considered here are reported in Fig. 2.

From Fig. 2 we can see that the relative Young's moduli E_{M1}/E_{O1} and E_{M2}/E_{O2} generally increase with the increase of N and they are greatly influenced by the thickness-to-length ratio t_0/l_0. Compared with its corresponding equal-mass OAHH, the enhancements of the relative in-plane stiffness of the AMHH could be 1.5 times (for $t_0/l_0=0.1$ in Fig. 2c) or even more than 100 times (for $t_0/l_0=0.01$ in Fig. 2a). For $t_0/l_0=0.1,\ N_{\min}=N_{\max}=11$ (Fig. 2c). When t_0/l_0 is larger than 0.1, $N_{\min}$ will be larger than $N_{\max}$, the theory given in this section will be not valid anymore. So for the examples given in this section, the validation of the range for the thickness-to-length ratio is $t_0/l_0\leqslant 0.1$.

2.2. AMHH with Kagome honeycomb substructure

2.2.1. Basic theory

In this section, we study another kind of AMHH, namely, by replacing the cell walls of the OAHH with their equal mass isotropic Kagome honeycomb substructures (Fig. 3). Like that defined in Section 3.1, here the hierarchical length ratio, i.e., the ratio between l_k and $\min[h_0,l_0]$, is expressed as

$$\lambda=\frac{1}{n}=\frac{l_k}{l} \tag{20}$$

in which

$$\begin{cases} l_k=\frac{l_0}{n_1}=\frac{h_0}{n_2} \\ \frac{n_2}{n_1}=\frac{h_0}{l_0} \end{cases} \tag{21}$$

$$n=\begin{cases} n_1 & h_0/l_0>1 \\ n_2 & h_0/l_0<1 \end{cases} \tag{22}$$

$$l=\begin{cases} l_0 & h_0/l_0>1 \\ h_0 & h_0/l_0<1 \end{cases} \tag{23}$$

l_k is the side length of triangles in Kagome cells, and n_1 and n_2 are respectively the numbers of length l_k lying on the middle line of the oblique (with length l_0) and vertical (with length h_0) AMHH cell walls. From Fig. 3c and d it is easy to see that n_1 and n_2 are even numbers. According to the equal-mass principle, we can find $t_0l_0-1/\left(2\sqrt{3}\right)t_0^2=3\times\left(t_kl_k-\sqrt{3}/2t_k^2\right)M$, which gives

$$\frac{t_k}{l_k}=\frac{1}{\sqrt{3}}\left[1-\sqrt{1-\frac{2\sqrt{3}}{3\lambda^2M}\frac{t_0}{l}\left(1-\frac{1}{2\sqrt{3}}\frac{t_0}{l}\right)}\right] \tag{24}$$

where

$$\frac{t_0}{l}=\begin{cases} \frac{t_0}{l_0} & \frac{h_0}{l_0}>1 \\ \frac{t_0}{l_0}\frac{1}{h_0/l_0} & \frac{h_0}{l_0}<1 \end{cases} \tag{25}$$

and M is the total number of triangles in one AMHH cell wall with length l and it relates to n and N by (See Appendix B)

$$M=2N(n-N)\quad\left(1\leqslant N\leqslant\frac{n}{2}\right) \tag{26}$$

in which N is the number of the Kagome representative cells (e.g., in Fig. 3b, $N=1$) away from the middle line of the AMHH cell walls.

Also, here we suppose that both the cell walls of the AMHH and the Kagome honeycomb substructures are Euler beams. Then, the precondition $t_k/l_k<0.2$ holds, which gives $N_{\min}$, the lower bound of N:

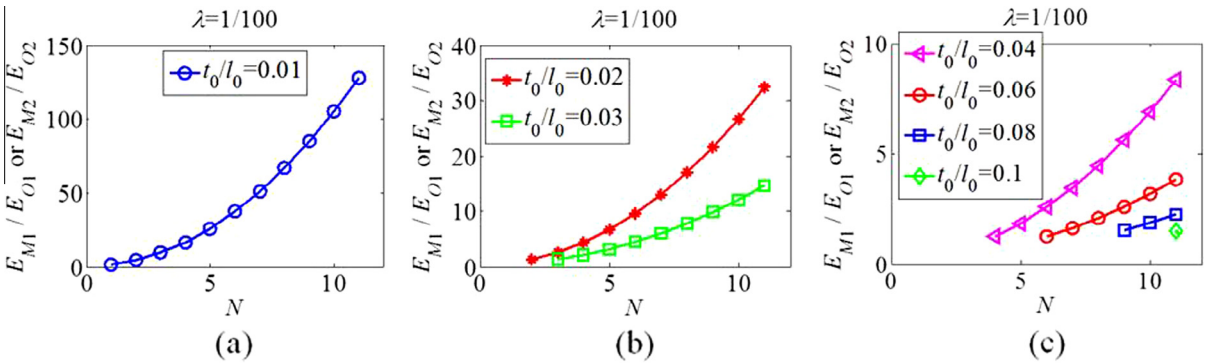

Fig. 2. The relative Young's modulus E_{M1}/E_{O1} or E_{M2}/E_{O2} vs. N for different t_0/l_0: (a) $t_0/l_0=0.01$; (b) $t_0/l_0=0.02,\ 0.03$; (c) $t_0/l_0=0.04,\ 0.06,\ 0.08,\ 0.1$.

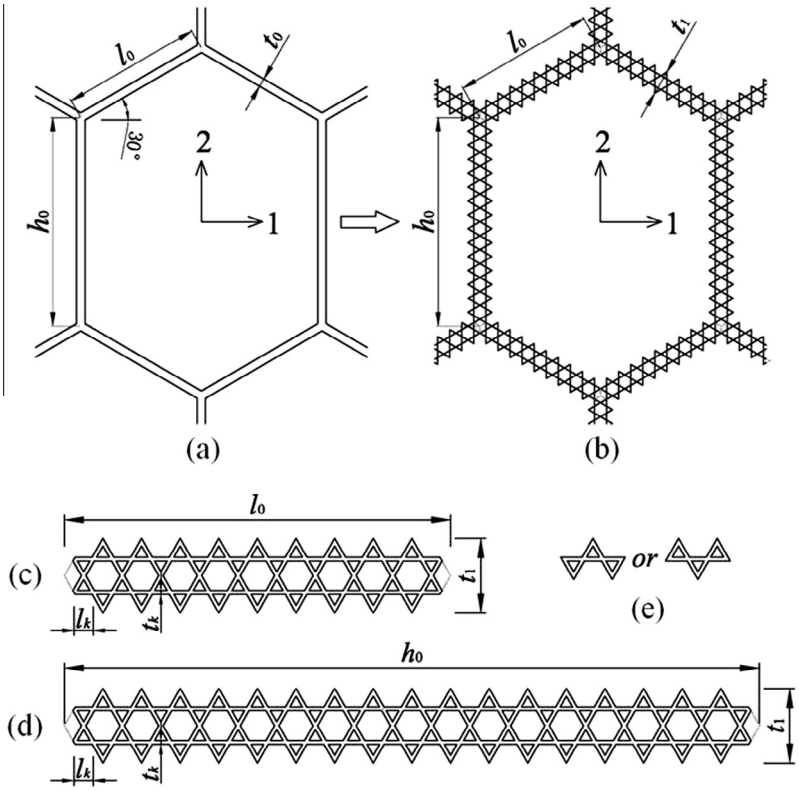

Fig. 3. Schematics of (a) the OAHH with 120° angles between the jointed cell walls; (b) the tailorable AMHH with Kagome honeycomb substructures; (c) amplification of the oblique Kagome lattice cell wall with length l_0 in (b); (d) amplification of the vertical Kagome lattice cell wall with length h_0 in (b); (e) the representative cells for the Kagome honeycomb.

$$N_{\min} = ce\left[\frac{n - n\sqrt{1 - \frac{100}{3(10-\sqrt{3})}\frac{t_0}{l}\left(1 - \frac{1}{2\sqrt{3}}\frac{t_0}{l}\right)}}{2}\right] \tag{27}$$

Note that Eq. (27) may give $N_{\min} = 0$, in this case $N_{\min} = 1$.

On the other hand, from the geometrical analysis of Fig. 3c or d we get the cell wall thickness of the AMHH with Kagome honeycomb substructures

$$t_1 = 2N\left(\sqrt{3}l_k\right) + 2t_k \tag{28}$$

that is

$$\frac{t_1}{l} = 2\left(\sqrt{3}N + \frac{t_k}{l_k}\right)\lambda \tag{29}$$

Then from the Euler beam assumption $t_1/l < 0.2$, we obtain $N_{\max}$, the upper bound of N:

$$N_{\max} = fl\left[\frac{1}{10\sqrt{3}\lambda}\right] = fl\left[\frac{n}{10\sqrt{3}}\right] \tag{30}$$

Using the same definitions of E_s, E_{O1}, E_{O2}, E_{M1}, E_{M2} given in Section 2.1.1 and defining E_k as the Young's modulus of the Kagome honeycomb substructures, we find [34]:

$$\frac{E_k}{E_s} = \frac{1}{\sqrt{3}}\frac{t_k}{l_k} \tag{31}$$

The expressions for E_s, E_{O1}, E_{O2}, E_{M1}, E_{M2} are the same to those given in Section 2.1.1, here we don't repeat them anymore. Combining Eq. (31) with Eqs. (14)–(17) gives the relative Young's moduli of the AMHH with Kagome honeycomb substructures in the principal directions 1 and 2:

$$\frac{E_{M1}}{E_{O1}} = \frac{E_{M2}}{E_{O2}} = \frac{1}{\sqrt{3}}\frac{t_k}{l_k}\left(\frac{t_1}{l_0}\right)^3 \Big/ \left(\frac{t_0}{l_0}\right)^3 \tag{32}$$

in which t_1/l_0 in Eq. (32) still has the form shown in Eq. (18).

2.2.2. Effects of N and t_0/l_0 on the relative Young's moduli

To explicitly show how to design the AMHH structure with Kagome honeycomb substructure under given parameters h_0/l_0 and t_0/l_0 of the OAHH structure and to investigate the effects of N and t_0/l_0 on the relative Young's moduli E_{M1}/E_{O1} and E_{M2}/E_{O2}, we try to consider the same examples for the AMHH with triangular honeycomb substructure given in Section 2.1.2, i.e., the parameters are still $h_0/l_0 = 1.5$, $t_0/l_0 = 0.01, 0.02, 0.03, 0.04, 0.06, 0.08, 0.1$.

Since $h_0/l_0 = 1.5 > 1$, here we could also define $n_1 = 100$, $n_2 = h_0/l_0 n_1 = 150$ (See Eqs. (21) and (22)). Then Eqs. (22), (23) and (20) give $n = n_1 = 100$, $l = l_0$ and $\lambda = 1/n = l_k/l_0 = 1/100$, respectively. Through these parameters we obtain $N_{\max} = 5$ by Eq. (30) and the lower bound $N_{\min}$ for each t_0/l_0 could be obtained by Eq. (27).

Through Eq. (27) we find that $N_{\min} = N_{\max} = 5$ when $t_0/l_0 = 0.04$ and $N_{\min}$ will be larger than $N_{\max}$ when $t_0/l_0 > 0.04$. This means that the validation of the range of the thickness-to-length ratio for the example considered here is $t_0/l_0 \leqslant 0.04$. Then, the relative Young's moduli E_{M1}/E_{O1} and E_{M2}/E_{O2} vs. N for $t_0/l_0 = 0.01, 0.02, 0.03, 0.04$ are calculated and they are reported in Fig. 4.

Comparing Fig. 4 with Fig. 2, it is apparent that the Kagome honeycomb substructures could also greatly improve the in-plane stiffness of the AMHH structure, 10 times (for $t_0/l_0 = 0.04$ in Fig. 4b) or even more than 100 times (for $t_0/l_0 = 0.01$ in Fig. 4a). It is also apparent that the applicability of

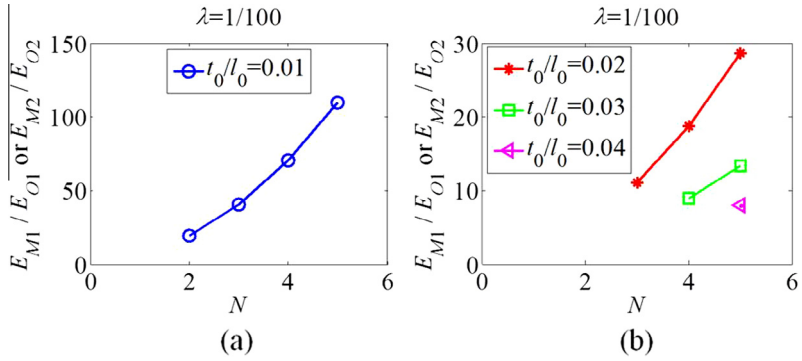

Fig. 4. The relative Young's modulus E_{M1}/E_{O1} or E_{M2}/E_{O2} vs. N for different t_0/l_0: (a) $t_0/l_0 = 0.01$; (b) $t_0/l_0 = 0.02,\ 0.03,\ 0.04$.

the range of the thickness-to-length ratio t_0/l_0 for the triangular honeycomb substructures ($t_0/l_0 \leqslant 0.1$) could be much larger than that for the Kagome honeycomb substructures ($t_0/l_0 \leqslant 0.04$). In fact, comparing the geometrical layouts of the triangular and Kagome honeycomb substructures, it is not difficult to imagine that under the same given parameters of the OAHH the applicability of the range of the thickness-to-length ratio t_0/l_0 for the triangular honeycomb substructures is about 2 times larger than that for the Kagome honeycomb substructures.

3. AMHH corresponding to the OAHH with angles between the jointed cell walls different from 120°

In this section, we study the AMHH corresponding to the OAHH with angles between the jointed cell walls different from 120°, i.e., the angles between the oblique cell walls and the horizontal line (the principal direction 1) are not equal to 30° (see Fig. 5a). In this case, the layouts of the AMHH structures are not geometrically compatible, i.e., the connection between the honeycomb substructure cell walls is not geometrical occlusive naturally (Fig. 5b). The substructure cell walls need to be tailored to connect each other.

3.1. Basic theory

Since in Section 2 it is shown that the applicability of the range of the thickness-to-length ratio t_0/l_0 for the triangular honeycomb substructures is larger than that for the Kagome honeycomb substructures, here we only consider the AMHH with isotropic triangular honeycomb substructures (Fig. 5). Defining the angles between the oblique walls and the horizontal line (the principal

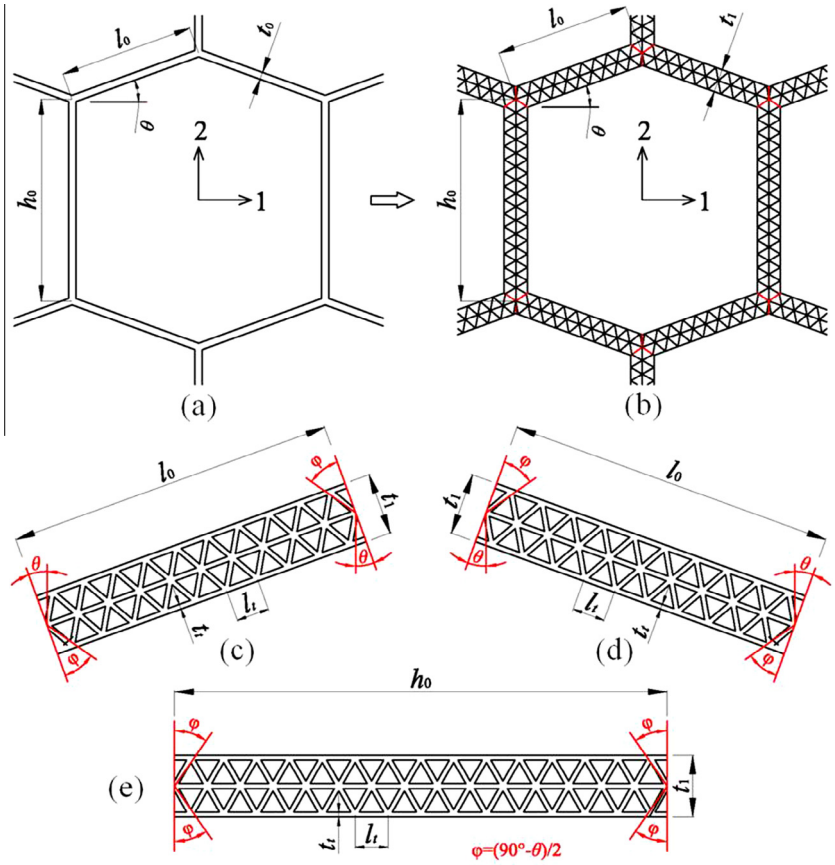

Fig. 5. Schematics of (a) the OAHH with angles between the jointed cell walls different from 120°; (b) the tailorable AMHH with isotropic triangular honeycomb substructures; (c) amplification of the right oblique (the vertical direction is taken as the reference line) triangular lattice cell wall with length l_0 in (b); (d) amplification of the left oblique triangular lattice cell wall with length l_0 in (b); and (e) amplification of the vertical triangular lattice cell wall with length h_0 in (b).

direction 1) as $\theta(\theta \neq 30^{\circ})$ and taking the vertical direction as the reference line, the right oblique, the left oblique and the vertical triangular lattice cell walls of the AMHH are constructed by cutting the four corners through θ and $\varphi(\varphi = (90^{\circ} - \theta)/2)$ shown in Fig. 5c–e, respectively. From Fig. 5c–e it is easy to see that the tailored right oblique, left oblique and vertical triangular lattice cell walls are geometrically occlusive.

For the AMHH corresponding to the OAHH with angles between the jointed cell walls different from 120°, the design of n_1, n_2, λ and l is the same as that given in Section 2.1 but we appropriately use the equal-mass principle by (See Appendix C)

$$t_0 l = 3 \times \frac{1}{2}\left(t_t l_t - \frac{\sqrt{3}}{2} t_t^2\right) M + 2 \times \frac{t_t}{2} l \tag{33}$$

in which $M = 4Nn$. Rearranging Eq. (33) gives

$$\frac{t_t}{l_t} = \frac{2}{3\sqrt{3}}\left[\frac{3}{2} + \frac{1}{4N} - \sqrt{\left(\frac{3}{2} + \frac{1}{4N}\right)^2 - \frac{3\sqrt{3}n}{4N}\frac{t_0}{l}}\right] \tag{34}$$

Then, the precondition $t_t/l_t < 0.2$ gives $N_{\min}$, the lower bound of N:

$$N_{\min} = ce\left[\frac{5(5nt_0/l - 1)}{30 - 3\sqrt{3}}\right] \tag{35}$$

The cell wall thickness of the AMHH structure, t_1, and the upper bound of N, $N_{\max}$, are also the same as Eqs. (10) and (12).

Again, using the same definitions for E_s, E_t, E_{O1}, E_{O2}, E_{M1} and E_{M2} given in Section 2.1.1, here we find [33]:

$$\frac{E_t}{E_s} = \frac{2}{\sqrt{3}}\frac{t_t}{l_t} \tag{36}$$

$$\frac{E_{O1}}{E_s} = \frac{\cos\theta}{(h_0/l_0 + \sin\theta)\sin^2\theta}\left(\frac{t_0}{l_0}\right)^3 \tag{37}$$

$$\frac{E_{M1}}{E_t} = \frac{\cos\theta}{(h_0/l_0 + \sin\theta)\sin^2\theta}\left(\frac{t_1}{l_0}\right)^3 \tag{38}$$

$$\frac{E_{O2}}{E_s} = \frac{h_0/l_0 + \sin\theta}{\cos^3\theta}\left(\frac{t_0}{l_0}\right)^3 \tag{39}$$

$$\frac{E_{M2}}{E_t} = \frac{h_0/l_0 + \sin\theta}{\cos^3\theta}\left(\frac{t_1}{l_0}\right)^3 \tag{40}$$

where t_1/l_0 has the form of Eq. (18).

Combining Eqs. (36)–(38) and Eqs. (36), (39), (40) gives the relative Young's moduli in the principal directions 1 and 2 of the AMHH corresponding to the OAHH with angles between the jointed cell walls different from 120°:

$$\frac{E_{M1}}{E_{O1}} = \frac{E_{M2}}{E_{O2}} = \frac{2}{\sqrt{3}}\frac{t_t}{l_t}\left(\frac{t_1}{l_0}\right)^3 \Big/ \left(\frac{t_0}{l_0}\right)^3 \tag{41}$$

Apparently, Eq. (41) is the same as Eqs. (19) and (32) and is independent of θ.

3.1.1. Effects of N and t_0/l_0 on the relative Young's moduli

The same as Section 2.1, here we still consider the following examples with parameters $h_0/l_0 = 1.5$, $t_0/l_0 = 0.01$, 0.02, 0.03, 0.04, 0.06, 0.08, 0.1 to investigate the effects of N and t_0/l_0 on the relative Young's moduli E_{M1}/E_{O1} and E_{M2}/E_{O2}. And still the following parameters, $n_1 = 100$, $n_2 = h_0/l_0 n_1 = 150$, $n = n_1 = 100$, $l = l_0$ and $\lambda = 1/n = l_t/l_0 = 1/100$, are used since $h_0/l_0 = 1.5 > 1$. Calculating the lower bound $N_{\min}$ and $N_{\max}$ for each t_0/l_0 by Eqs. (35) and (12), the relative Young's moduli E_{M1}/E_{O1} and E_{M2}/E_{O2} vs. N for all the t_0/l_0 considered here are shown in Fig. 6.

Similar to Fig. 2, in Fig. 6 it is also obvious that the triangular honeycomb substructures could greatly increase the in-plane stiffness of the AMHH corresponding to the OAHH with angles between the jointed cell walls different from 120°, by 1.5 times (for $t_0/l_0 = 0.1$ in Fig. 6c) or even more than 100 times (for $t_0/l_0 = 0.01$ in Fig. 6a). The validation of the range for the thickness-to-length ratio could also reach to $t_0/l_0 = 0.1$.

4. Conclusions

In this paper, the anisotropic multifunctional hierarchical honeycomb (AMHH) is proposed by replacing the solid cell walls of the original anisotropic hexagonal honeycomb (OAHH) with the equal mass isotropic substructures, triangular or Kagome honeycombs. Two kinds of AMHH structures are constructed. One corresponds to the OAHH with 120° angles between the jointed cell walls and the other one corresponds to those with angles between the jointed cell walls different from 120°. The in-plane stiffness of these two kinds of AMHH is analytically studied with the help of Euler beam theory. Results show that the triangular honeycomb substructures could greatly increase the in-plane stiffness of the AMHH by 1.5 times or even more than 100 times, depending on the thickness-to-length ratio t_0/l_0 of the oblique cell wall, which is related to the relative density, of the OAHH. And the applicability of the range of the thickness-to-length ratio t_0/l_0 for the triangular honeycomb substructures is larger than that for the Kagome honeycomb substructures. For the former one, the validation of the range for the thickness-to-length ratio t_0/l_0 could reach to 0.1. The theory present in this paper could provide new strategy for

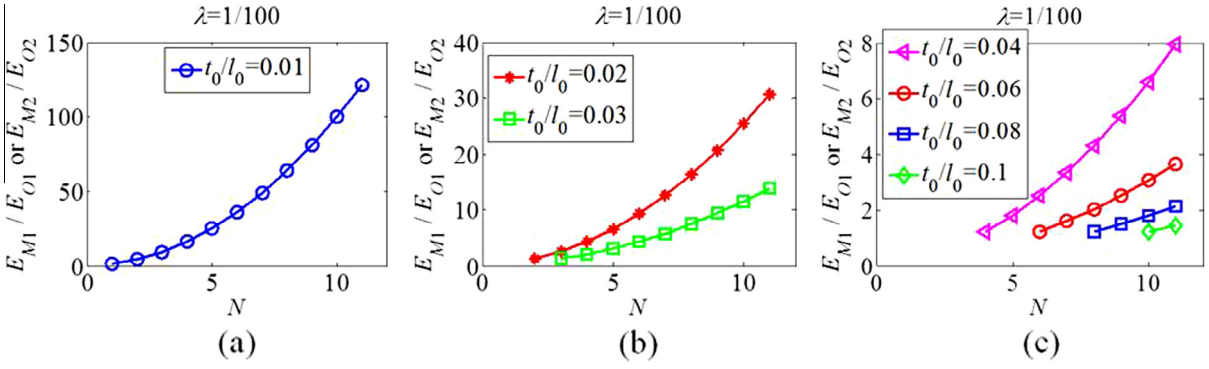

Fig. 6. The relative Young's modulus E_{M1}/E_{O1} or E_{M2}/E_{O2} vs. N for different t_0/l_0: (a) $t_0/l_0 = 0.01$; (b) $t_0/l_0 = 0.02$, 0.03; (c) $t_0/l_0 = 0.04$, 0.06, 0.08, 0.1.

the design of the new tailorable anisotropic hierarchical honeycomb materials for multifunctional applications, e.g., the metallic AMHH could be used as the core of the light weight sandwich panels for thermal isolation, heat dissipation or vibration control in civil engineering, mechanical engineering, aerospace engineering and so on.

Acknowledgments

The work is supported by the Seed Foundation of Tianjin University (Grant No. 1405), 973 Program (No. 2014CB049000) and the fund (Grant No. GZ1408) from State Key Laboratory of Structural Analysis for Industrial Equipment, Dalian University of Technology. NMP acknowledges support from the European Research Council, ERC Ideas Starting Grant No. 279985 "BIHSNAM", from ERC Proof of Concept Grant No. 619448 "REPLICA2" and No. 632277 "KNOTOUGH", from the Graphene FET Flagship ("Graphene-Based Revolutions in ICT And Beyond" – Grant agreement No. 604391), and from the Autonomous Province of Trento (Graphene PAT WP10, code 81017).

Appendix A. AMHH cell wall with triangular honeycomb substructures corresponding to the OAHH with 120° angles between the jointed cell walls

Fig. A.1 schematically shows the cell wall (with length $l = \min[h_0, l_0]$) of the AMHH with triangular honeycomb substructures corresponding to the OAHH with 120° angles between the jointed cell walls. Different from the isotropic MHH with triangular honeycomb substructures proposed in reference [32], here the cell wall with length $l(l = \min[h_0, l_0])$ is chosen as the base cell wall for the design of t_t and l_t, which will assure the Euler beam assumptions for both the AMHH cell walls with length h_0 and l_0. Once the cell wall length l is confirmed, the relation between M, n and N will be the same as that given in Appendix B of reference [32]:

$$M = 2N(2n - N) + \frac{2}{3}(n - N) \quad (1 \leqslant N \leqslant n) \tag{A.1}$$

Appendix B. AMHH cell wall with Kagome honeycomb substructures corresponding to the OAHH with 120° angles between the jointed cell walls

Fig. B.1 schematically shows the cell wall (with length $l = \min[h_0, l_0]$) of the AMHH with Kagome honeycomb substructures corresponding to the OAHH with 120° angles between the jointed cell walls. Different from the isotropic MHH with Kagome honeycomb substructures proposed in reference [32], here the cell wall with length $l(l = \min[h_0, l_0])$ is chosen as the base cell wall for the design of t_k and l_k, which will assure the Euler beam assumptions for both the AMHH cell walls with length h_0 and l_0. Once the cell wall length l is confirmed, the relation between M, n and N will be the same as that given in Appendix C of reference [32]:

$$M = 2N(n - N) \tag{B.1}$$

Appendix C. AMHH cell wall with triangular honeycomb substructures corresponding to the OAHH with angles between the jointed cell walls different 120°

Fig. C.1 schematically shows the cell wall (with length $l = \min[h_0, l_0]$) of the AMHH with triangular honeycomb substructures corresponding to the OAHH with angles between the jointed cell walls different from 120°. Different from the design of the AMHH with triangular honeycomb substructures corresponding

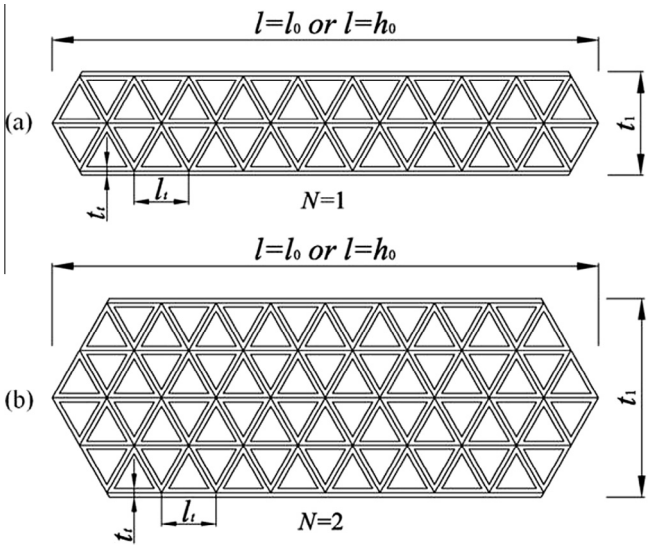

Fig. A.1. Schematics of the AMHH cell walls with length l ($l = l_0$ if $h_0/l_0 > 1$; $l = h_0$ if $h_0/l_0 < 1$) in Fig. 1b: (a) $N = 1$; (b) $N = 2$.

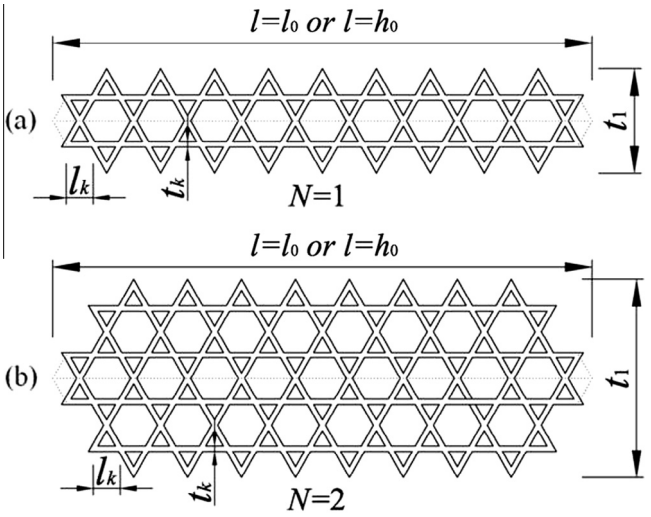

Fig. B.1. Schematics of the AMHH cell walls with length l ($l = l_0$ if $h_0/l_0 > 1$; $l = h_0$ if $h_0/l_0 < 1$) in Fig. 3b: (a) $N = 1$; (b) $N = 2$.

to the OAHH with 120°angles between the jointed cell walls given in Appendix A, here the equal mass principle directly equals the mass of the cell walls with length l and thickness t_0 in OAHH (Fig. C.1a) to that of the AMHH cell walls with length l and thickness t_1 (Fig. C.1b or c). After t_t, l_t and t_1 are calculated, according to the Euler beam assumption the topology of both the AMHH cell walls with length h_0 and l_0 will be confirmed. Then, tailoring the right oblique, left oblique and vertical AMHH cell walls through θ and φ shown in Fig. 5b–e and connecting them gives the AMHH structure with triangular honeycomb substructures corresponding to the OAHH with angles between the jointed cell walls different from 120° (Fig. 5a).

The hierarchical length ratio is $\lambda = 1/n$. M is the total number of the half-thickness triangular cells in one sub-structure cell wall. N is the number of triangular lattice cells away from the middle line of the AMHH cell walls. From Fig. C.1b and c, it is very simple to recursively get the relationship between M, n and N:

$$M = 4Nn \tag{C.1}$$

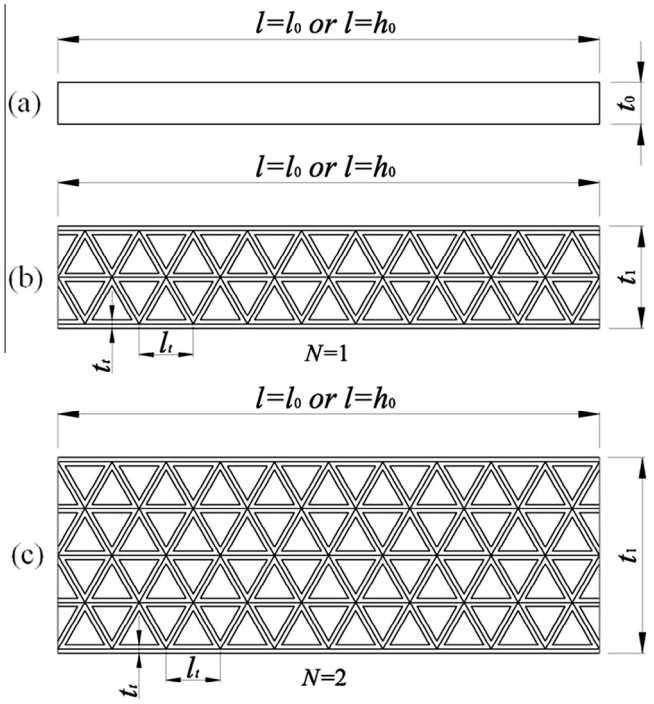

Fig. C.1. Schematics of the AMHH cell walls with length l ($l = l_0$ if $h_0/l_0 > 1$; $l = h_0$ if $h_0/l_0 < 1$) in Fig. 5b: (a) $N = 1$; (b) $N = 2$.

References

[1] Lu LX, Sun YP, Wang ZW. Critical buckling load of paper honeycomb under out-of-plane pressure. Packag Technol Sci 2005;18:141–50.
[2] Lu TJ. Heat transfer efficiency of metal honeycombs. Int J Heat Mass Transf 1999;42(11):2031–40.
[3] Gu S, Lu TJ, Evans AG. On the design of two-dimensional cellular metals for combined heat dissipation and structural load capacity. Int J Heat Mass Transf 2001;44(11):2163–75.
[4] Vosa R, Barrett R. Pressure adaptive honeycomb: a new adaptive structure for aerospace applications. Sensors and smart structures technologies for civil, mechanical and aerospace systems 2010, Proc. of SPIE, 7647, 76472B; 2010. doi: 10.1117/12.847031.
[5] Vosa R, Barrett R, Romkes A. Mechanics of pressure adaptive honeycomb. J Intell Mater Syst Struct 2011;22(10):1041–55.
[6] Ko WL. Heat shielding characteristics and thermostructural performance of a superalloy honeycomb sandwich thermal protection system (TPS). NASA/TP-2004-212024; 2004.
[7] Takemiya H. Field vibration mitigation by honeycomb WIB for pile foundations of a high-speed train viaduct. Soil Dyn Earthq Eng 2004;24:69–87.
[8] Jung WY, Aref AJ. A combined honeycomb and solid viscoelastic material for structural damping applications. Mech Mater 2003;35:831–44.
[9] Thompson RW, Matthews FL. Load attachments for honeycomb panels in racing cars. Mater Design 1995;16(3):131–50.
[10] Shin KB, Lee JY, Cho SH. An experimental study of low-velocity impact responses of sandwich panels for Korean low floor bus. Compos Struct 2008;84:228–40.
[11] Zinno A, Fusco E, Prota A, Manfredi G. Multiscale approach for the design of composite structures for train application. Compos Struct 2010;92:2208–19.
[12] Wadley HNG. Multifunctional periodic cellular metals. Philos Trans R Soc A 2006;364(1838):31–68.
[13] Lakes R. Materials with structural hierarchy. Nature 1993;361:511–5.
[14] Pugno N. Mimicking nacre with super-nanotubes for producing optimized super-composites. Nanotechnology 2006;17(21):5480–4.
[15] Gao H. Application of fracture mechanics concepts to hierarchical biomechanics of bone and bone-like materials. Int J Fract 2006;138:101–37.
[16] Pugno N, Carpinteri A. Design of micro-nanoscale bio-inspired hierarchical materials. Philos Mag Lett 2008;88(6):397–405.
[17] Carpinteri A, Pugno N. Mechanics of hierarchical materials. Int J Fract 2008;150:221–6.
[18] Zhao Q, Kreplak L, Buehler MJ. Hierarchical structure controls nanomechanical properties of vimentin intermediate filaments. PLoS ONE 2009;4(10):e7294.
[19] Fratzl P, Weinkamer R. Nature's hierarchical materials. Prog Mater Sci 2007;52:1263–334.
[20] Pugno N, Chen Q. In plane elastic properties of hierarchical cellular solids. Eng Proced, Phys Eng 2011;10:3026–31.
[21] Chen Q, Pugno N. Modeling the elastic anisotropy of woven hierarchical tissues. Compos Part B: Eng 2011;42(7):2030–7.
[22] Chen Q, Pugno N. Mechanics of hierarchical 3-D nanofoams. Europhys Lett 2012;97:26002.
[23] Chen Q, Pugno N. In-plane elastic buckling of hierarchical honeycomb materials. Eur J Mech A/Solids 2012;34:120–9.
[24] Chen Q, Pugno N. Competition between in-plane buckling and bending collapses in nano-honeycombs. Europhys Lett 2012;98:16005.
[25] Chen Q, Huang S. Mechanical properties of a porous bioscaffold with hierarchy. Mater Lett 2013;95:89–92.
[26] Chen Q, Pugno NM. Bio-mimetic mechanisms of natural hierarchical materials: a review. J Mech Behav Biomed Mater 2013;19:3–33.
[27] Sun YT, Pugno N. Hierarchical fibers with a negative Poisson's ratio for tougher composites. Materials 2013;6(2):699–712.
[28] Taylor CM, Smith CW, Miller W, Evans KE. The effects of hierarchy on the in-plane elastic properties of honeycombs. IJSS 2011;48(9):1330–9.
[29] Ajdari A, Jahromi BH, Papadopoulos J, Nayeb-Hashemi H, Vaziri A. Hierarchical honeycombs with tailorable properties. IJSS 2012;49:1413–9.
[30] Oftadeh R, Haghpanah B, Papadopoulos J, Hamouda AMS, Nayeb-Hashemi H, Vaziri A. Mechanics of anisotropic hierarchical honeycombs. Int J Mech Sci 2014;81:126–36.
[31] Sun YT, Pugno N. In plane stiffness of multifunctional hierarchical honeycombs with negative Poisson's ratio sub-structures. Compos Struct 2013;106:681–9.
[32] Sun YT, Chen Q, Pugno N. Elastic and transport properties of the tailorable multifunctional hierarchical honeycombs. Compos Struct 2014;107:698–710.
[33] Gibson LJ, Ashby MF. Cellular solids, structures and properties. 2nd ed. Cambridge: Cambridge University Press; 1997.
[34] Wang AJ, McDowell DL. In-plane stiffness and yield strength of periodic metal honeycombs. J Eng Mater Technol 2004;126(2):137–56.